Available online at www.sciencedirect.com
ScienceDirect
Journal of Hazardous Materials 154 (2008) 417–425
Journal of Hazardous Materials
www.elsevier.com/locate/jhazmat

Mineral phases of weathered and recent electric arc furnace dust

Fernanda Machado Martins [a], José Manoel dos Reis Neto [b], Carlos Jorge da Cunha [a,*]

[a] *Laboratório de Química Mineral Aplicada, Departamento de Química, Universidade Federal do Paraná (UFPR), CP 19081, CEP 81.530.000, Curitiba-PR, Brazil*
[b] *Laboratório de Análise de Minerais e Rochas (LAMIR–UFPR), CEP 81.530.000, Curitiba-PR, Brazil*

Received 24 July 2007; received in revised form 11 October 2007; accepted 11 October 2007
Available online 18 October 2007

Abstract

A weathered and a recent sample of electric arc furnace dust (EAFD), generated in a southern Brazilian steel industry, were characterized by X-ray fluorescence spectroscopy (XFA), powder X-ray diffraction (XRD), thermogravimetric analysis (TG), scanning electron microscopy (SEM) with energy dispersive spectroscopy (EDS) probe and Fourier transform infrared spectroscopy (FTIR). A quantitative phase composition model, that accounts for the observed data and for the physico-chemical conditions of formation, was postulated for each material. One sample, in the form of a wet paste, was collected from the lowest part of a landfill and corresponds to a weathered material whereas the other sample was collected from the top portion of the landfill and corresponds to a recently produced material. The dominant cations present in both samples are iron, zinc and lead with minor amounts of manganese, calcium and silicon. The dominant mineralogical phases identified in both materials are Magnetite, Franklinite and Zincite. The recent sample has Laurionite whereas the weathered sample has Hydrocerussite and Hydrozincite.

Keywords: Analysis; EAFD; Elemental; Infrared; TG; Phases; SEM

1. Introduction

The world raw steel production on 2006 was 1200 billion metric tonnes [1], Latin America contributed with 4% of this production being Brazil the biggest producer. The current annual Brazilian raw steel produced with electric arc furnace (EAF) is between 7 and 8 million metric tonnes. Paraná State produces some 400 thousand tonnes of raw steel per year [2].

The steel plant under study is located in Paraná State and uses EAF process in which iron scrap is the main source of iron and pig iron is a secondary source. Oxygen is injected during the melting process and act on decarburization and on the burning of natural gas and coal. Dolomitic or calcitic lime is added to make slag. An extra energy input is obtained from the combustion of natural gas and pulverized coal. The electrodes are made of carbon and are slowly consumed in the process. The fused material in the EAF reaches temperatures of 1600 °C, the molten steel is then poured in a ladle furnace for refining. Lime, to make slag, and alloying elements are added in this stage. The molten refined steel is directed to a continuous molding system where the ingots are water cooled and cut. The EAF processing generates gases, volatile organic compounds, slag and particulates known as EAF dust or simply EAFD. The EAFD is directed to a bag filter system that is periodically washed with water generating a sludge. In past plant operations this wet sludge was placed in a hazardous waste landfill. Nowadays this sludge is directed to a pelletizer that considerably reduces the humidity and material volume. No chemicals are added to make the EAFD pellets that are being landfilled on top of the sludge. The estimated generation of EAFD in this plant is 9.6 thousand tonnes/year.

According to Brazilian standards [3], the EAFD is classified as a dangerous residue due to the potential leaching of toxic metal ions. Its disposal in controlled landfills is the main form of final destination in Brazil.

Recent work has been dedicated to the characterization of EAFD from different steel plants with focus on the solid EAFD [4,5] or on its leaching products [6,7]. Various applications for the EAFD are been suggested such as the study of its vitrification product [8], the recovery of zinc and iron [9–16], soil fertilization [17], recycling to the EAF [18–21], incorporation in cement [22,23] and incorporation in glass [24].

* Corresponding author. Tel.: +55 41 3361 3181; fax: +55 41 3361 3186.
E-mail address: cjdcunha@quimica.ufpr.br (C.J.d. Cunha).

0304-3894/$ – see front matter © 2007 Elsevier B.V. All rights reserved.
doi:10.1016/j.jhazmat.2007.10.041

According to a recent study [25] the EAFD formation takes place in two steps: first, the emission of dust "precursors" (vapors, metal droplets, and solid particles) inside the furnace; second, the conversion of those precursors into dust by agglomeration and physico-chemical transformations. Out of the five possible emission mechanisms evaluated the two most important were found to be the projection of fine metal droplets by bursting of CO bubbles (coming from the decarburization of the steel bath) and volatilization at the hot spots in the arc zone, in the oxygen jet zone and in the CO bubbles. The direct fly-off of solid particles from the EAF feed, such as coal powder and lime powder depend on operational conditions and may even be absent in optimized furnaces. The projection of metal droplets at the impact points of the arc and at the impact points of the oxygen jet were found to be an unlikely mechanism because the large particles projected return to the molten bath. The so generated air-borne precursors can undergo physical transformations in their way out of the EAF and into the filtration system such as condensation of the vapors, rapid solidification of the fine metal droplets, in-flight agglomeration and coalescence of dust particles [25].

In the present work a recent and a weathered EAFD sample were collected, from a landfill of a southern Brazilian steel plant, and were characterized by means of an integrated approach, developed by our research team, that takes into account diffractometry, electron microscopy, spectroscopy, thermal analysis and the physico-chemical conditions of residue formation. This integrated approach has recently been applied to various types of industrial residues [26] including four residues of a pulp and paper plant [27]. The authors hope that this methodology can be useful to help finding industrial uses for this material and to improve EAF process control. This is the first work, to the authors' knowledge, to characterize a recent and a weathered EAFD sample generated in the same steel mill.

2. Experimental

2.1. Sampling

Sampling of the two residues was performed according to a Brazilian standard [28]. The weathered material, representative of past operations of the industry, was collected from the lowest part of a landfill, whereas the recently generated material was collected from the topmost part of the landfill.

2.2. Sample preparation and analysis

Each sample, of approximately 2 kg of residue, was dried at 70 °C for 48 h, ground and divided with a riffle splitter to obtain a 15 g sample. This sample was milled, in a Herzog vibration grinding mill, for one minute, to get a powder suitable for XFA, XRD, TG and FTIR measurements and for the calcination experiment. The calcination experiment was performed in new porcelain crucibles at 1000 °C for three hours. The calcined samples were cooled slowly inside a desiccator with silica gel.

The XFA measurements were performed in a PHILIPS, model PW 2400 at LAMIR-UFPR laboratory. The powdered samples were mixed with wax and pressed to form a pellet. The results were interpreted with the software semi-Q PHILIPS and were normalized to 100%. This normalization takes into account the loss on ignition (LOI) estimated as the total mass loss, below 550 °C, measured in the TG experiment.

The powder XRD was performed in the dried samples, referred to as "in natura" from now on, and in the calcined samples. The diffractometer used was a SHIMADZU, Lab-X model XRD-6000 (radiation Cu Kα, θ/2θ scans, 40 kV and 30 mA) located at the Chemistry Department-UFPR. The diffractograms were interpreted with the aid of data banks [29–31].

Simultaneous TG and DTA data were obtained on a thermal analyser Mettler TGA/STDA851 at the Lamir Laboratory of the Geology Department-UFPR. A sample weighing between 50 and 110 mg was placed in a 70 mL aluminum crucible and heated, under an oxygen flux of 50 L min^{-1}, from room temperature up to 550 °C at a rate of 5 °C min^{-1}. The experiments were repeated under nitrogen.

FTIR spectra were collected on a FTIR BOMEM model MB-100, of the Chemistry Department-UFPR, on KBr pellets, between 4000 and 400 cm^{-1} with a 4 cm^{-1} resolution and 32 scans.

In order to obtain good quality SEM-BES (scanning electron microscopy, backscattered electron) images and reliable EDS (Energy Dispersive Spectroscopy) data the powdered samples were imobilized in a special resin in a procedure adapted from the ones used for biological samples. The dried powder sample was mixed with liquid propylene oxide and with a Poly Bed 812 resin (chloromethyl oxiran polymer) with a polymerization catalyst. The propylene oxide promotes the embedding of the powder particles in the resin matrix. The mixture was then placed in a polyethylene cone and left to cure in an oven at 70 °C for 72 h. After cooling to room temperature the tip of the cone was cut with a clean blade exposing a surface with the embedded sample that was flushed with deionized water and wet polished with a fine sand paper (1200, silicon carbide). After hot air drying, the sample was mounted on the SEM sample holder and placed inside the equipment. The thickness of the sample was kept below 6 mm and no metalization was used. The surface, so prepared, was observed with the electron microscope SEM JEOL, model JSM-6360, in low vacuum, with an EDS probe thermonoran at the CEM laboratory of the SCB-UFPR.

The pH of the residues was determined according to the SW 846 method 9045D. The pH meter used was a Schott Handylab 1.

3. Results and discussion

3.1. EAFD characterization

3.1.1. Elemental analysis

The elemental chemical composition of the weathered and recent EAFD samples can be seen in Table 1. The weathered sample and the recent sample have Fe, Zn and Pb as the major electropositive elements, intermediate amounts of Mn, Ca and Si and trace amounts of other elements. A comparison between EAFD from different origins reveals a significant variation in the

Table 1
Composition (mass%) of recent and weathered EAFD

XRF elemental analysis	Weathered (mass%)	Weathered (mmol)	Recent (mass%)	Recent (mmol)
Fe	39.32	704.1	36.46	652.8
Zn	23.51	359.6	28.47	435.5
Pb	4.57	22.0	4.05	19.5
Mn	2.39	43.5	1.95	35.4
Ca	1.91	47.7	1.73	43.2
Si	1.69	60.2	1.12	40.0
Cl	0.36	10.1	1.48	41.6
Cu	0.34	5.4	0.35	5.5
Al	0.30	11.2	0.11	4.0
Cr	0.30	5.8	0.00	0.0
P	0.27	8.8	0.26	8.5
K	0.23	6.0	0.77	19.7
Mg	0.20	8.4	0.23	9.6
Sn	0.20	1.7	0.23	2.0
Ti	0.11	2.2	0.07	1.4
Ba	0.10	0.7	0.00	0.0
Sr	0.08	0.9	0.06	0.7
Ni	0.04	0.7	0.04	0.7
I	0.01	0.1	0.21	1.6
Cd	0.01	0.1	0.07	0.6
S	0.00	0.0	0.42	13.1
O (of fixed oxides)[a]	21.18	1323.7	19.62	1226.1
TG assigned mass loss				
H_2O from dehydrations[b]	1.18 (1)			
CO_2 and H_2O[c]	1.03 (2)			
Dehydration of Laurionite			0.98 (1)	
Organic matter burning	0.73 (3)		1.33 (2 + 3)	
Loss on ignition (<550 °C)[d]	2.94		2.31	
Total	100.06		100.00	

The values were normalized from XFA and "loss on ignition" from TG data and are given in a dry basis. The numbers in parenthesis correspond to the thermal events identified in the DTA curves in Fig. 2.

[a] Oxygen present in the fixed oxides estimated from the oxide of each element. It does not account for the oxygen of water and carbon dioxide lost on ignition.

[b] Dehydration of $Ba(OH)_2{\cdot}8H_2O$, dehydroxilation of $Cr(OH)_3$, other dehydrations.

[c] CO_2 and H_2O from hydrocerussite and hydozincite and H_2O from clay dehydroxylation.

[d] Loss on ignition is the sum of all losses in the assigned thermal events.

elemental composition. The EAFD samples studied here have Fe, Zn, Pb, Mn, Ca, Cr and Ni percentages close to those related by Leclerc et al. [14], whereas the Fe percentage in the weathered sample is close to that reported by Sofilic et al. [4], the percentages of Zn in both samples are close to that reported by Yamada and Hara [10]. The percentage of Pb in both samples agrees with that reported by Sekula et al. [11]. These variations in compositions are mainly due to the different types of iron and steel scrap consumed in the EAF, to the type of steel being produced and to particular operations performed during the steel production. The EAFD zinc originates form the galvanized iron scrap, lead comes from the paint present in the scrap pieces, manganese, chromium, silicon, nickel, phosphorus and titanium are present in steel alloys, chromium may also come from metalized steel pieces, calcium, magnesium, barium, potassium and strontium originate from the calcitic and dolomitic lime used in the EAF, copper comes from wiring mixed with the scrap and tin comes from solder. Al is commonly present in the zinc layer of galvanized iron and steel. In the weathered EAFD Al may also come from environmental clay contamination.

Both EAFD samples are basic, the pH test revealed 8.50 for the weathered sample and 7.85 for the recent sample.

3.1.2. XRD analysis

The diffractograms of the weathered and recent EAFD samples, in natura, can be seen in Fig. 1. The major phase identified in both in natura samples were spinels present as

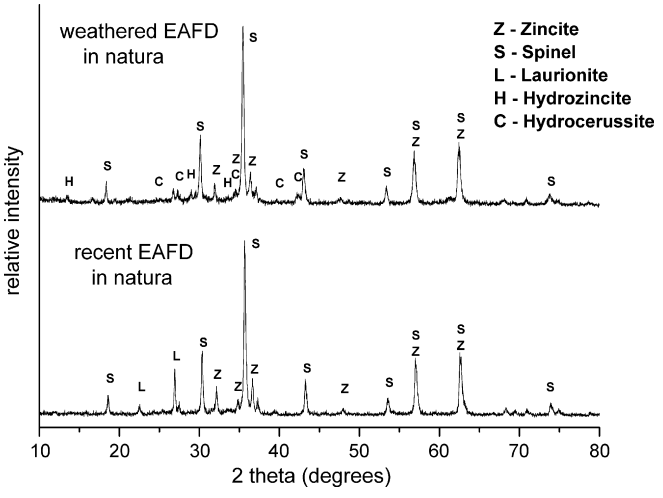

Fig. 1. X-ray powder diffractograms of weathered and recent EAFD samples.

a solid solution or a mixture of Magnetite ($Fe^{II}Fe^{III}{}_2O_4$) and Franklinite ($Zn^{II}Fe^{III}{}_2O_4$). Cromite ($Fe^{II}Cr^{III}{}_2O_4$) is also possible in the weathered sample. The presence of aluminum oxide, chromium(III) oxide and aluminum manganese oxide cannot be ruled out because they have Spinel like XRD pattern. In the recent sample the dominant spinel is Magnetite possibly in a solid solution with small amounts of Franklinite. Zincite (ZnO) was identified in both "in natura" samples. Laurionite (Pb(OH)Cl) was identified as the main lead species in the recent "in natura" sample. The weathered sample also presents Hydrocerussite ($Pb_3(CO_3)_2(OH)_2$) and Hydrozincite ($Zn_5(OH)_6(CO_3)_2$). Laurionite and Hydrocerussite are typical weathering products of lead [32–35] and Hydrozincite is a known weathering product of zinc [36]. The presence of titanium dioxide, suspected to be present in all four samples, could not be ascertained due to the superimposition of its two most intense diffraction peaks with those of spinel.

The overall data interpretation, to be given in Section 4, indicates the presence of clay minerals in the weathered sample but the presence of this phase could not be unambiguously confirmed in the diffractogram due to the superimposition of its diffraction peaks with those of the more abundant phases. In agreement with the present assignments Sekula et al. [11], Leclerc et al. [13], Sofilic et al. [4] and Machado et al. [5], report the presence of Franklinite, Zincite and iron oxides in EAFD.

The diffractograms of both EAFD calcined samples (Fig. S1, Supplementary material) displayed spinel and Zincite diffraction peaks. The differences between the diffractograms of in natura and calcined samples can be interpreted assuming the following thermal processes during the calcination: (1) Hydrozincite decomposes into carbon dioxide, water and zincite, (2) Hydrocerussite decomposes into carbon dioxide, water and lead oxide (PbO), (3) Laurionite decomposes into lead oxide and lead chloride ($PbCl_2$), (4) both lead oxide and lead chloride sublime, (5) zinc oxide, and spinels (Magnetite, Franklinite, other less abundant spinels) react to form a single Spinel phase where all

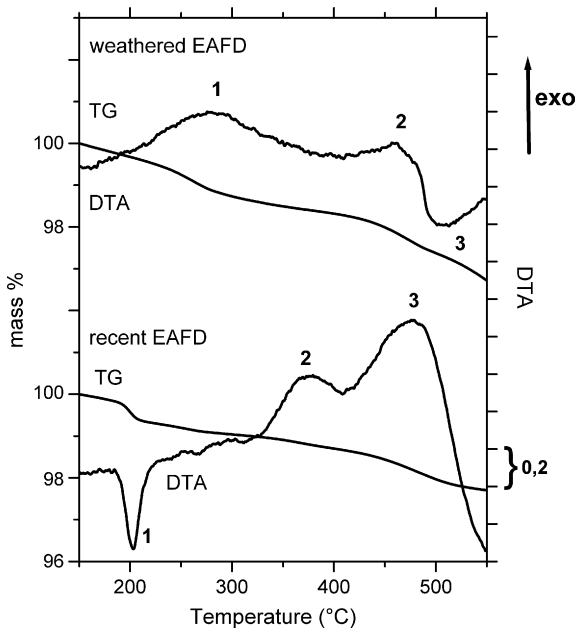

Fig. 2. TG and DTA curves of weathered and recent EAFD samples in oxygen atmosphere.

Fe atoms are present as Fe(III). The absence of Hematite in the calcined samples is an indication that Magnetite reacted to form a new spinel phase instead of being converted to Hematite.

3.1.3. Thermal analysis TG/DTA

Thermogravimetric and differential thermal analysis curves for the weathered and recent EAFD samples, in oxygen atmosphere, between 150 and 550 °C can be seen in Fig. 2. The curves obtained in nitrogen atmosphere can be seen in Fig. S2 (Supplementary material). Below 150 °C both samples loose humidity and above 550 °C they loose lead compounds by sublimation. In order to avoid contamination of the equipment with lead oxide, the samples were not heated above 550 °C.

Table 2
Phase assignment for the weathered and recent EAFD samples, both in natura, mass% estimated on a dry basis

Residue	Phase formula	Phase name	Mass %
Weathered EAFD in natura	$ZnFe_2O_4$	Franklinite	43.3
	ZnO	Zincite	14.6
	Fe_3O_4	Magnetite	26.6
	$Pb_3(CO_3)_2(OH)_2$	Hydrocerussite	5.7
	$Al_2Si_2O_5(OH)_4$	Clay minerals	0.37
		Organic matter	0.73
		Hydroxides, Hydrozincite, unidentified phases	8.70
Total			100
Recent EAFD in natura	$ZnFe_2O_4$	Franklinite	52.5
	ZnO	Zincite	17.7
	Fe_2O_3	Magnetite	16.8
	Pb(OH)Cl	Laurionite	5.1[a]
		Organic matter	1.33
		Unidentified phases	6.57
Total			100

[a] Estimated from XFA-Pb. The amount of Laurionite estimated from TG data is 28.3%. This value is considered to be an overestimation due to errors in the determination of small mass variations associated with the respective thermal event.

In both samples the observed mass loss is below 3%. From TG and DTA data, from the comparison between the XRD experiments performed on "in natura" and on "calcined" samples and from literature data, the thermal processes, within this temperature range, were assigned (Table 1). In the recent sample, the dehydroxilation of Laurionite (Pb(OH)Cl) is assigned to process 1 [37,38]. In the weathered sample, the pyrolysis of Hydrocerussite ($Pb_3(CO_3)_2(OH)_2$) [39] and Hydrozincite ($Zn_5(OH)_6(CO_3)_2$) [40–42] and clay dehydroxilation [43,44] are assigned to process 2. Since the thermal decomposition of Hydrocerussite depends on its origin [45] its assignment has a high degree of uncertainty. In both samples a reaction between Zincite and Magnetite, generating Franklinite, is expected to occur below 1000 °C but the exact temperature range in which this reaction occurs has not yet been identified, nevertheless this temperature is presumed to be above 550 °C [46], the highest temperature set in the experiments. Organic matter, if present, should undergo pyrolysis, in nitrogen atmosphere and burn, in oxygen atmosphere. Organic matter burning was assigned to process 3 in the weathered and to processes 2 and 3 in the recent sample [47–50]. Process 1, in the weathered sample, is assigned to dehydrations and dehydroxilations of unidentified compounds. Some of these compounds may be hydrated barium hydroxide [51] and chromium(III) hydroxide [52] but no confirmation of these phases were obtained with the other characterization techniques used here. The given assignments of thermal processes take into account that pyrolysis, dehydrations and dehydroxilations are endothermic and that the franklinite synthesis and the organic matter burning are exothermic as told from DTA data. Due to the overlap of thermal processes and to the small magnitude of mass variations, the assigned mass losses given in Table 2 may have a large error.

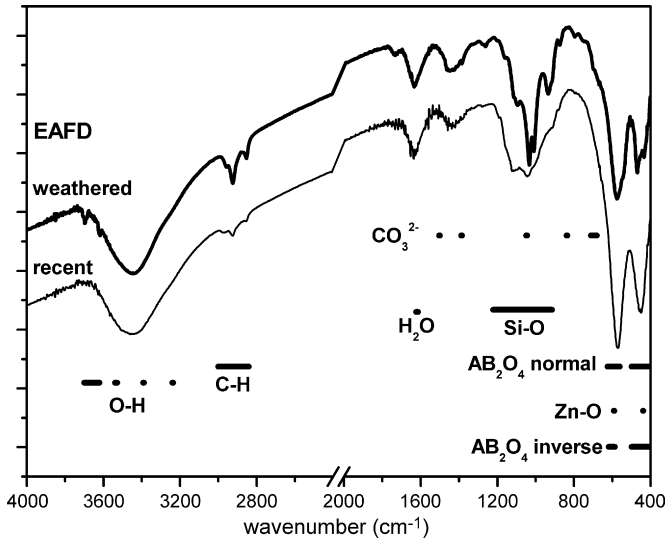

Fig. 3. FTIR spectra of weathered and recent EAFD samples prepared as KBr pellets.

Mikhail et al. [8] also performed TG analysis on EAFD samples from stainless steel and carbon steel plants but their results do not quite match the ones obtained for the EAFD samples analysed here.

3.1.4. FTIR spectra

The infrared spectra of both EAFD, in natura, samples can be seen in Fig. 3. Both spectra present a broad band, around 3460 cm^{-1} due to the O–H stretch of hydrogen bonded water. The O–H stretch bands of hydroxy groups of Laurionite [53], Hydrocerussite [33] and Hydrozincite [38] are not clearly iden-

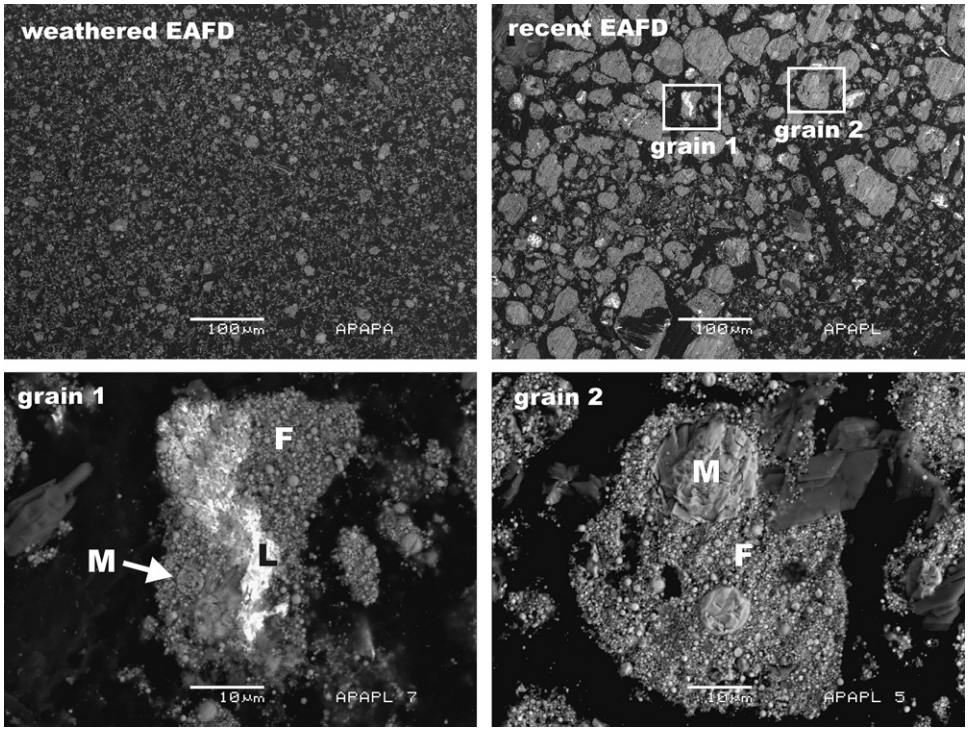

Fig. 4. SEM micrographs of weathered and recent samples (top images) and of grains 1 and 2 of the recent sample in magnified view (bottom images).

tified in the spectra and may be hidden below the strong broad band. The weathered sample also presents O–H stretch vibrations at 3694 and 3620 cm^{-1}, typical of clay minerals [54]. Both spectra display a band near 1640 cm^{-1} assigned to a vibration of the water molecule. The bands near 1440 and 1040 cm^{-1}, are assigned to carbonate (CO_3^{2-}) vibrations of Hydrocerussite [33] and Hydrozincite [38]. The intense bands in the region from 1100 to 932 cm^{-1} are assigned to Si–O vibrations [54]. The bands located at 574, 465 and 433 cm^{-1} are assigned to vibrations of simple oxides and spinels (AB_2O_4) [55]. In both spectra, the bands near 2900 cm^{-1}, are assigned to C–H stretch of aliphatic carbon chain indicating the presence of organic matter. The weathered sample also has bands at 1730 and 1260 cm^{-1}, characteristic of esthers [56], indicating a possible presence of polyester in the material. Low molecular weight esthers are ruled out because the sample is dried at 80 °C overnight prior to KBr pellet preparation. In the spectrum of the recent EAFD it is possible that the band located around 1120 cm^{-1} is due to a sulphate (SO_4^{2-}) vibration, being the other strong sulphate vibration, expected around 617 cm^{-1} [57], superimposed with a stronger spinel vibrational band. No sulphate is expected in the weathered sample since no sulfur was detected in the XFA.

3.1.5. SEM-EDS analysis

SEM micrographies of both EAFD samples, in the same resolution, can be seen in Fig. 4. The weathered sample has smaller grain size distribution than that of the recent sample as expected from the weathering action. The grains in the recent sample display various forms and many have more than one phase. Two representative grains of the recent sample are shown in detail in Fig. 4. Each grain is composed of aggregates of spherulitic granules characteristic of fly ashes [58] whose EDS elemental analysis points to a Franklinite phase. The phases with Fe, Zn and O as major elements were assigned to Franklinite (F), those with Pb, O and Cl as major elements were assigned to Laurionite (L) whereas those with Fe and O as major elements were assigned to Magnetite (M). The Zincite phase was not clearly identified in none of the grains analysed with EDS spectra. These phase assignments take into account the phases identified in the XRD interpretation. Due to the fine-grained structure of the weathered sample and to the spatial resolution of the EDS probe it was not possible to unambiguously assign its grain composition.

3.2. Physico-chemical conditions of EAFD formation

3.2.1. Recent EAFD

The agreggates of spherulitic granules (composed of spinels) observed in Fig. 4 indicate that the granules have undergone sinterization during the fly off from the molten metal to the bag filter. The spherical shape of the granules indicates they have been formed from the liquid state. In the EAF the temperature of the molten metal is around 1600 °C and the surrounding atmosphere is rich in oxygen. Metal droplets are mainly generated from the bursting of decarburization CO bubbles and from the volatilization at the EAF hot spots [25]. Iron droplets, zinc droplets and iron zinc droplets, are oxidized during the fly off towards the bag filter originating the major phases identified in the EAFD, Spinels (Magnetite and Franklinite) and Zincite. Despite the fact that the XRD diffraction peaks of the Spinel phase Maghemite reasonably match those observed in the XRD diffractogram of the sample, it was not considered as a likely one because it is not the stable iron oxygen phase under the EAF conditions according to phase diagrams. In Fig. 4 it can be seen that the diameters of Magnetite granules are micrometric whereas those of Franklinite granules are submicrometric. Other less abundant metals, eventually present in the droplets, may also be similarly oxidized. Airborne particles of calcium and magnesium oxides, formed during lime pyrolysis, and airborn particles of unburnt coal are also part of the EAFD. After EAFD cooling to room temperature, in the bag filter, the calcium and magnesium oxides absorb moisture from the air leading to the formation of calcium and magnesium hydroxides that, in turn, absorb carbon dioxide leading to the formation of calcium and magnesium carbonates. No short-term weathering or other chemical reactions of coal particles are anticipated to occur. After the EAFD washing process and pellet making process further chemical oxidation may take place together with the precipitation of Laurionite generated from lead oxide, water and the chloride anion present in the washing water. The aspect of the assigned Laurionite phase in Fig. 4 is consistent with the proposed chemical precipitation mechanism. Salts present in the washing water will also become part of the pellets because, in the pellet making process, the excess water evaporates leaving no free liquid. The water was supplied by local water works facility and should contain minor amounts of treatment chemicals such as calcium hydroxide, sodium orthopolyphosphate and sodium fluorosilicate. The amounts of these chemicals in EAFD pellets is assumed to be very small because fluoride and sodium were not even detected in the XRF spectral analysis.

3.2.2. Weathered EAFD

The main morphological difference between the recent and the weathered EAFD is the particle agglomeration. The agglomerates of sperulitic granules observed in the recent EAFD are no longer seen in the weathered material. It is probable that the weathering of the surface of the granules during the years has ended up eroding the sintered granules loosing them form one another. Regardless of the morphology the major mineral phases present in the recent EAFD, Spinels (Magnetite and Franklinite), are also present in the weathered EAFD. The absence of Hematite, as told from XRD data, indicates that the Magnetite phase has not even partially been oxidized to Hematite suggesting the aqueous solution in the landfill is reducing. The Laurionite phase, easily observable in the recent EAFD, gave rise to Hydrocerussite, through weathering, including dissolution and reprecipitation from the carbonated rain water trapped in the landfill. The Hydrocerussite phase was not detected under the microscope resolution used meaning that its grains must be very fine (below hundredths of micrometers). The Zincite phase has partially been converted to Hydrozincite as told from XRD diffraction. This conversion is expected to occur through dissolution of Zincite and

reprecipitation of Hydrozincite from the carbonated rain water in the landfill. The organic matter, present in the recent sample, is absent in the weathered material, as told from TG data, indicating it has been destroyed through weathering. The weathering of the organic matter is thought to be of microbiological nature. From the inspection of predominance diagrams both Hydrozincite [59] and Hydrocerussite [32] solid phases are stable under the conditions prevailing in the landfill, that is, aqueous solution at a slightly reducing potential, containing dissolved atmospheric carbon dioxide at slightly basic pH.

4. Mineral phase quantification

Taking into account all qualitative and quantitative data collected, a major phase composition model was stablished for each material (Table 2). The percentage of some phases were estimated from TG data and/or from XFA data. If the mass variation for a thermal event can be precisely measured from TG data, meaning that it has well defined plateaus before and after the event, the TG data is highly reliable. Due to the nature of the XFA measurements the smaller the concentration of a given element, the higher the error in its quantification. In the present work the thermal events measured in the TG experiments have very low corresponding mass variations meaning that the associated errors are high. For that reason preference was given to estimations based on XFA data. If a more precise, but far more expensive, quantification is needed, atomic emission spectroscopy (AES) could be used. Phase quantification can also be made from numerical manipulation of XRD data if suitable standards are available.

The following specific assumptions were made for the estimations in Table 2.

4.1. Recent EAFD sample

The estimation of the amount of Franklinite, Zincite and Magnetite is based on the percentages of iron and zinc determined from XFA. It is assumed that the molar proportion between the Franklinite zinc and the Zincite zinc is 1/1 [14]. The amount of Magnetite iron is estimated subtracting the amount of Franklinite iron from the total iron. The amount of Laurionite was estimated from two data: (1) assuming that all XFA-Pb is in the form of Laurionite; (2) assuming that the mass loss of process 1 in the TG experiment corresponds solely to water lost by Laurionite. The amount left to reach 100% was estimated to be due to unidentified substances.

The pH of the sample is compatible with the presence of Laurionite [32].

4.2. Weathered EAFD sample

The estimation of the amount of Franklinite, Zincite and Magnetite is made in a similar way to that of the recent sample. However in the weathered sample, a small part of Zn is in the form of Hydrozincite (impossible to estimate from the available data). The amount of Hydrocerussite was estimated from the total Pb (XFA-Pb). The amount of clay was estimated assuming that all Al (XFA-Al) is in the form of Kaolinite ($Al_2Si_2O_5(OH)_4$). The amount left to reach 100% was estimated to be due to Hydrozincite, hydroxides and unidentified substances.

The pH of the sample is compatible with the presence of Hydrocerussite and Hydrozincite [32].

5. Conclusions

A recent and a weathered sample of EAFD, generated in the same steel mill, were characterized by means of an integrated approach and a mineral phase composition model was estimated for each sample. The major chemical composition of the weathered and recent EAFD samples are similar being Fe, Zn and Pb the most dominant electropositive elements.The major phases present in both samples are also similar being spinels (Franklinite and Magnetite) and Zincite the most dominant ones. The recent sample has Laurionite as the main lead bearing phase. The weathered material has two hydroxicarbonates, Hydrozincite and Hydrocerussite, typical weathering products of zinc and lead. The pH of the samples is compatible with the presence of the assigned phases. Clay and some type of ester (or polyester) are also part of the weathered sample. Calcination of the samples, at 1000 °C for 3 h, promotes the decomposition of the hydroxicarbonates into oxides, the sublimation of lead oxide, the oxidation of iron(II) and the reaction between zincite and iron oxides to form Franklinite. The recent sample displays agglomerates of spherulitic granules being the submicrometric ones composed of Franklinite and the micrometric ones composed of Magnetite. The observed lead bearing phase in the electron micrographies of recent sample is consistent with the proposed precipitation of Laurionite. In the weathered sample the granules are completely loose and well mixed as told from the electron micrographies. During the course of the present work it was realized that the thermal treatment of EAFD may be a useful source of synthetic Franklinite, a rare mineral, whose applications in materials science are appealing. The prospect use of this EAFD as a source of synthetic Franklinite is currently being evaluated.

The authors hope that this integrated approach be useful to help finding industrial uses for EAFD and to improve the EAF process control.

Supplementary material

TG curves for both EAFD samples run under nitrogen atmosphere and XRD diffractograms for both calcined EAFD samples are available as supplementary material.

Acknowledgements

The authors would like to acknowledge the following persons and institutions for their intellectual and/or material help: CME-UFPR: Regina F. Piontek, Sergio Tokunaga and Rosangela Borges; LAMIR-UFPR: Dr. Eleonora Vasconcellos, Dr.

Joaniel Munhoz Martins, Dr. José Eduardo Gardolinski, Luciane Lemos do Prado, Rodrigo Secchi, Elisiane Roper Pescini, Francielen Pereira da Silva and Carlos Lara Ribeiro; Chemistry Department - UFPR: Dr. Fernando Wypych, Dr. Sueli Drechsel and Dr. Aldo Zarbin; Biology Department - UFPR: Dr. Ciro Alberto Ribeiro. Gerdau Guaíra: Elias Sater, Carolina Greter. LACTEC: Dr. Gabriel Sousa and Dr. Paulo Brixel.

Appendix A. Supplementary data

Supplementary data associated with this article can be found, in the online version, at doi:10.1016/j.jhazmat.2007.10.041.

References

[1] Mineral Commodity Summaries—USGS-2007. Available at http://minerals.usgs.gov/minerals/pubs/mcs/.
[2] Instituto Brasileiro de Siderurgia-IBS. Available at http://www.ibs.org.br.
[3] ABNT—Associação Brasileira de Normas Técnicas, NBR 10.004, Resíduos Sólidos – Classificação, 2004.
[4] T. Sofilic, A. Rastovcan-Mioc, S. Cerjan-Stefanovic, V. Novosel-Radovic, M. Jenko, Characterization of steel mill electric-arc furnace dust, J. Hazard. Mater. B 109 (2004) 59–70.
[5] J.G.M.S. Machado, F.A. Brehm, C.A.M. Moraes, C.A. Santos, A.C.F. Vilela, J.B.M. Cunha, Chemical, physical, structural and morphological characterization of the electric arc furnace dust, J. Hazard. Mater. B 136 (2006) 953–960.
[6] G. Laforest, J. Duchesne, Characterization and leachability of electric arc furnace dust made from remelting of stainless steel, J. Hazard. Mater. B 135 (2006) 156–164.
[7] A.J.B. Dutra, P.R.P. Paiva, L.M. Tavares, Alkaline leaching of zinc from electric arc furnace steel dust, Miner. Eng. 19 (2006) 478–485.
[8] S.A. Mikhail, A.M. Turcotte, J. Aota, Thermoanalytical study of EAF dust and its vitrification product, Thermochim. Acta 287 (1996) 71–79.
[9] M. Siebenhofer, H. Schweiger, K. Lorber, Upgrading of zinc from galvanic sludge and steel furnace dust, Sep. Sci. Technol. 32 (1–4) (1997) 759–773.
[10] S. Yamada, Y. Hara, Simultaneous recovery of zinc and iron from electric arc furnace dust with a coke-packed bed smelting-reduction process, Iron Steel Eng. 75 (8) (1998) 64–67.
[11] R. Sekula, A. Selinger, M. Wróbel, Electric arc furnace dust treatment: investigation on mechanical and magnetic separation methods, Waste Manage. Res. 19 (2001) 271–275.
[12] S. Isosaki, T. Furukawa, R. Takahashi, H. Sasamoto, The tecnology for direct separation and recovery of iron from EAF exhaust gases, Rev. Metall. Paris 99 (1) (2002) 31–39.
[13] N. Leclerc, E. Meux, J.M. Lecuire, Hydrometallurgical recovery of zinc and lead from electric arc furnace dust using mononitrilotriacetate anion and hexahydrated ferric chloride, J. Hazard. Mater. B 91 (2002) 257–270.
[14] N. Leclerc, E. Meux, J.M. Lecuire, Hydrometallurgical extraction of zinc from zinc ferrites, Hydrometallurgy 70 (2003) 175–183.
[15] J.M. Yoo, B.S. Kim, J.C. Lee, M.S. Kim, C.W. Nam, Kinetics of the volatilization removal of lead in electric arc furnace dust, Mater. Trans. 46 (2) (2005) 323–328.
[16] T. Havlík, B.V. Souza, A.M. Bernardes, I.A.H. Schneider, A. Miskufová, Hydrometallurgical processing of carbon steel EAF dust, J. Hazard. Mater. B 135 (2006) 311–318.
[17] R. Melloni, F.A.M. Silva, F.M.S. Moreira, A.E.F. Neto, Pó de forno de aciaria elétrica na microbiota do solo e no crescimento de soja, Pesqui. Agropecu. Bras. 36 (12) (2001) 1547–1554.
[18] A.F. López, A. López-Delgado, Enhancement of electric arc furnace dust by recycling to electric arc furnace, J. Environ. Eng Asce. 128 (12) (2002) 1169–1174.
[19] M.C. Mantovani, C. Takano, P.M. Buchler, Electric arc furnace dust-coal composite pellet: effects of pellet size, dust composition, and additives on swelling and zinc removal, Ironmaking Steelmaking 29 (4) (2002) 257–265.
[20] J. Peng, B. Peng, D. Yu, M.T. Tang, J. Lobel, J.A. Kozinski, Volatilization of zinc and lead in direct recycling of stainless steel making dust, T. Nonferr. Met. Soc. 14 (2) (2004) 392–396.
[21] O. Ruiz, C. Clemente, M. Alonso, F.J. Alguacil, Recycling of an electric arc furnace flue dust to obtain high grade ZnO, J. Hazard. Mater. 141 (2007) 33–36.
[22] G. Laforest, J. Duchesne, Stabilization of electric arc furnace dust by the use of cementitious materials: ionic competition and long-term leachability, Cement Concrete Res. 36 (2006) 1628–1634.
[23] A.S. Vargas, A.B. Masuero, A.C.F. Vilela, Investigations on the use of electric-arc furnace dust (EAFD) in Pozzolan-modified Portland cement I (MP) pastes, Cement Concrete Res. 36 (2006) 1836–1841.
[24] P. Kavouras, T. Kehagias, I. Tsilika, G. Kaimakamis, K. Chrissafis, S. Kokkou, D. Papadopoulos, Th. Karakostas, Glass-ceramic materials from electric arc furnace dust, J. Hazard. Mater. A 139 (2007) 424–429.
[25] A.G. Guézennec, J.C. Huber, F. Patisson, P. Sessiecq, J.P. Birat, D. Ablitzer, Dust formation in electric arc furnace: birth of the particles, Powder Technol. 157 (2005) 2–11.
[26] F.M. Martins, Dissertação de Mestrado, Caracterização Química e Mineralógica de Resíduos Sólidos Industriais Minerais do Estado do Paraná. UFPR, Curitiba, 2006. Available at: http://hdl.handle.net/1884/5956.
[27] F.M. Martins, J.M. Martins, L.C. Ferracin, C.J. da Cunha, Mineral phases of green liquor dregs, slaker grits, lime mud and wood ash of a kraft pulp and paper mill, J. Hazard. Mater 147 (2007) 610–617.
[28] ABNT—Associação Brasileira de Normas Técnicas, NBR 10.007, Resíduos Sólidos – Amostragem, 2004.
[29] JCPDS-ICDD—International Center for Difraction Data, June 2001.
[30] MINCRYST—Crystallographic and Crystallochemical Database for Mineral and their Structural Analogues. Available at http://database.iem.ac.ru/mincryst/index.php.
[31] Webmineral—Mineralogy Database. Available at: http://www.webmineral.com.
[32] X. Cao, Q.M. Lena, M. Chen, D.W. Hardison Jr., W.G. Harris, Weathering of lead bullets and their environmental effects at outdoor shooting ranges, J. Environ. Qual. 32 (2003) 526–534.
[33] D. Dermatas, M. Dadachov, P. Dutko, N. Menounou, P. Arienti, G. Shen, Weathering of lead in fort irwin firing range soils, Global Nest: Int. J. 6 (2) (2004) 167–175.
[34] V. Ettler, Z. Johan, A. Baronnet, F. Jankovsky, C. Angilles, M. Mihaljevic, O. Sebek, L. Strnad, P. Bezdicka, Mineralogy of air-pollution-control residues from a secondary lead smelter: environmental implications, Environ. Sci. Technol. 39 (2005) 9309–9316.
[35] V. Ettler, M. Mihaljevic, O. Sebek, L. Strnad, Leaching of APC residues from secondary Pb metallurgy using single extraction tests: the mineralogical and the geochemical approach, J. Hazard. Mater. B 121 (2005) 149–157.
[36] H. Kucha, A. Martens, R. Ottenburgs, W. De Vos, W. Viaene, Primary minerals of Zn–Pb mining and metallurgical dumps and their environmental behavior at Plombières, Environ. Geol. 27 (1) (1996) 1–15.
[37] M.C. Ball, M.J. Casson, Thermal studies on lead(II) salts part 3. The decomposition of laurionite, lead(II) hydroxide chloride, Thermochim. Acta 17 (3) (1976) 361–367.
[38] S. Music, S. Popovic, M. Maljkovic, D. Dragcevic, Influence of synthesis procedure on the formation and properties of zinc oxide, J. Alloy Compd. 347 (2002) 324–332.
[39] A.M.A. Rehim, Thermal analysis of synthesis of wulfenite, J. Therm. Anal. Calorim. 46 (1996) 193–204.
[40] F.A. Sigoli, M.R. Davolos, M. Jafelicci Jr., Morphological evolution of zinc oxide originating from zinc hydroxide carbonate, J. Alloy Compd. 262 (3) (1997) 292–295.
[41] F.A. Sigoli, C.O.P. Santos, M. Jafelicci Jr., M.R. Davolos, Study of crystallite size and strain as a function of morphological evolution in zinc oxide powder obtained from hydroxycarbonate precursor, Powder Diffr. 16 (3) (2001) 153–159.

[42] N. Kanari, D. Mishra, I. Gaballah, B. Dupré, Thermal decomposition of zinc carbonate hydroxide, Thermochim. Acta 410 (2004) 93–100.
[43] S. Guggenheim, A.F. Koster Van Groos, Baseline studies of the clay minerals society source clays: thermal analysis, Clay Miner. 49 (5) (2001) 433–443.
[44] J.E. Gardolinski, F. Wypych, Esfoliação e hidratação da caulinita após intercalação com uréia, Quim. Nova. 24 (6) (2001) 761–767.
[45] N.J. Flemming, V.J. Lopata, B.L. Sanipelli, P. Taylor, Thermal decomposition of basic lead carbonates: a comparison of hydrocerussite and plumbonacrite, Thermochim. Acta 81 (1984) 1–8.
[46] F.J. Guaita, H. Beltrán, E. Cordoncillo, J.B. Carda, P. Escribano, Influence of the precursors on the formation and the properties of $ZnFe_2O_4$, J. Eur. Ceram. Soc. 19 (1999) 363–372.
[47] M. Tettamanti, E. Collina, M. Lasagni, D. Pitea, D. Grasso, C. La Rosa, Characterization of fly ash from municipal solid waste incinerators using differential scanning calorimetry, Thermochim. Acta 321 (1998) 133–141.
[48] M. Fan, R.C. Brown, Comparison of the loss-on-ignition and thermogravimetric analysis techniques in measuring unburned carbon in coal fly ash, Energ. Fuel. 15 (2001) 1414–1417.
[49] J. Payá, J. Monzó, M.V. Borrachero, E. Perris, F. Amahjour, Thermogravimetric methods for determining carbon content in fly ashes, Cement Concrete Res. 28 (5) (1998) 675–686.
[50] M.B. Fernandes, J.O. Skjemstad, B.B. Johnson, J.D. Wells, P. Brooks, Characterization of carbonaceous combustion residues. I. Morphological, elemental and spectroscopic features, Chemosphere 51 (2003) 785–795.
[51] A. Friedrich, M. Kunz, E. Suard, Temperature-dependent neutron powder diffr. study of the $Ba(OD)_2$ polymorphs: a new low-temperature phase, Acta Crystallogr. B B57 (2001) 747–758.
[52] R.A. Abdurakhmanov, Thermoanalytical and mössbauer spectroscopic studies of phase transformations of amorphous chromium hydroxide, J. Therm. Anal. Calorim. 33 (3) (1998) 857–863.
[53] H.D. Lutz, K. Beckenkamp, S.T. Peter, Laurionite-type M(OH)X (M = Ba, Pb; X = CI, Br, I) and Sr(OH)I. An IR and Raman spectroscopic study, Spectrochim. Acta 51A (5) (1995) 755–767.
[54] M.J. Wilson, Clay Mineralogy: Spectroscopic and Chemical Determinative Methods, first ed., Champman & Hall, London, 1994.
[55] G.C. Allen, M. Paul, Chemical characterization of transition metal spinel-type oxides by infrared spectroscopy, Appl. Spectrosc. 49 (4) (1995) 451–458.
[56] R.M. Silverstein, G.C. Bassler, T.C. Morril, Identificação Espectroscópica de Compostos Orgânicos, in: Guanabara Dois S.A. (Editora), third ed., John Wiley & Sons, Rio de Janeiro, 1979.
[57] K. Nakamoto, Infrared and Raman Spectra of Inorganic and Coordination Compounds, Chapter II-6, third ed., Wiley Interscience, New York, 1978, pp. 132–148.
[58] A.A. Landman, Aspects of solid-state chemistry of fly ash and ultramarine pigments, Ph.D. thesis, University of Pretoria, December, 2003. Available at http://upetd.up.ac.za/thesis/available/etd-06042004-062900/.
[59] W. Preis, H. Gamsjäger, (Solid+solute) phase equilibria in aqueous solution. XIII. Thermodynamic properties of hydrozincite and predominance diagrams for (Zn^{2+}+H_2O+CO_2), J. Chem. Thermodyn. 33 (7) (2001) 803–819.